Automatic Classification of Range-Time-Intensity Maps of Equatorial Spread-F

S.Palacios, M. Milla

Pontificia Universidad Católica Del Perú

e-mail: spalacios@pucp.edu.pe

Abstract

The equatorial spread F (ESF) is an ionospheric phenomenon related to plasma density irregularities at F-region heights. In Peru, the Jicamarca radar operating in the JULIA (Jicamarca Unattended Long-term Investigations of the Ionosphere and Atmosphere) mode has been used to measure the coherent backscatter signals generated by the ESF for many years. The measured power is plotted in Range-Time-Intensity (RTI) maps, and the database of these observations is available in Madrigal. Different morphological patterns of the ESF (bottom-type, bottomside, radar plumes, and E-echo) can be identified in the RTI maps. This study automatically identifies and classifies the ESF patterns in the RTI power maps measured with JULIA. The classification is based on machine learning algorithms using open-source tools. In particular, the Random Forest (RF), Extreme Gradient Boosting (XGBoost), and Neural Networks (NN) techniques are tested. Statistical pattern information and upper atmospheric physical parameters are used as features for classification.

Data and Methodology

The data set used for this work was 127 RTI maps corresponding to January and July 2020. The methodology involved two stages: building training data, and training a model using RF, XGBoost and NN methods. Figure 1 illustrates the inputs and outputs of this stage.

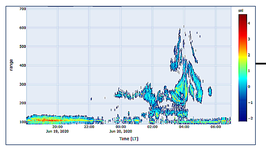

RTI map of echoes measured by JULIA on 19 June 2020

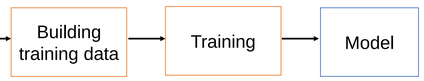

Figure 1: Methodology Block Diagram

Building training data

In this stage, we prepared the data sets to train and test the model. First, the RTI map was cleaned to avoid information unrelated to the ESF; therefore, minor artifacts were removed. Second, we manually labeled four patterns (bottom-type, bottom-side, radar plumes, and E-echoes) in each RTI map (Figure 2). These classifications follow the description in [1], [2], and [3]. Third, following the receipt in [4], we decreased the resolution of the RTI maps, where each power value corresponds to an average of a matrix made by a resolution of 15 min and 15 km in height (Figure 3). Then, statistical properties of the power that describe the texture content of a region were calculated. In total, six statistical properties were determined : mean, standard deviation, smoothness, the third moment of the power histogram, uniformity, and entropy. Finally, the measured power, the six statistical properties, the range, the time, vertical drift, horizontal drift, and the F10.7 solar flux index, were merged in a stack of 12 bands (Figure 4).

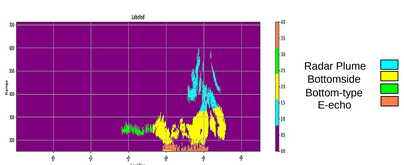

Figure 2: Manually label

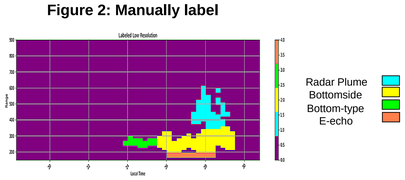

Figure 3: Low resolution

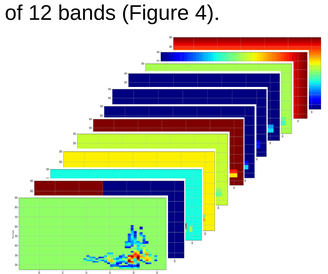

Figure 4: Stack of statistical textures, range, time, vertical drift, horizontal drift, F10.7, and power.

Training model

This stage involves training RF and XGBoost, and NN machine learning methods. We installed Scikit-Learn, and TensorFlow libraries to run the methods. The data set generated in the previous stage (Table 1) was divided into 2/3rd for training and 1/3rd for testing. The *K-fold cross-validation* feature was used, and we split the training set into five random subsets named folds. Then, the classification algorithm was trained and evaluated five times, picking a different fold for evaluation every time and training on the other four folds (Figure 5). Grid Search and Randomized Search were used to Fine-Tune the hyperparameters. Table 2 shows the setting parameters for each model.

Table 1: Total number of pixels per class.

Class	N. Of Pixels
Class 1: Radar Plume	6699
Class 2: Bottomside	9704
Class 3: Bottom-type	2793
Class 4: E-Echos	662

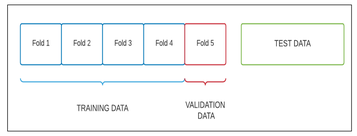

Figure 5: Train, Validation and Test data.

Table 2: Model configurations.

RF	XGBoost	NN
• Number of trees : 243 • Measure of the split quality: GINI • Max depth of the tree: 18 • Max features for best split: log2(12).	• Max depth of a tree: 9 • Learning rate: 0.2 • Number of boosting rounds: 150	• Learning rate: 0.0007 • Number of hidden layers: 3 • Number of neurons: 49 • Optimizer: Adam. • Activation: RELU. • Loss function: Categorical Crossentropy. • Number of epoch: 42.

Discussions and Conclusions

- Three machine learning algorithms are tested for ESF classification. XGBoost (93.41%) reach better results than Random Forest (91.75%) and Neural Network (84.87%) using the test data set. However, during the model application, Random Forest shows better results.
- On the other hand, we can observe that the models tend to predict radar plumes and bottomside. For instance, the NN application results are biased mainly to the bottomside class. This behavior is caused by the unbalanced data per class. Therefore, we need to add more bottom-type and E-echo data to improve the results.
- Future work will focus on using a Convolutional Neural Network since it considers the morphology of the data. Moreover, other upper atmospheric parameters at the equatorial region can be added as features.

References

[1] Hysell, D. L., & Burcham, J. D. (1998). JULIA radar studies of equatorial spread F. Journal of Geophysical Research, 103(A12), 29,155– 29,167. https://doi.org/10.1029/98JA02655.

[2] Hysell, D. L. (2000). An overview and synthesis of plasma irregularities in equatorial spread F. Journal of Atmospheric and Solar-Terrestrial Physics, 62 (12), 1037-1056. https://doi.org/10.1016/S1364-6826(00)00095-X

[3] Hysell, D. L., & Burcham, J. D. (2002). Long term studies of equatorial spread F using the JULIA radar at Jicamarca. Journal of Atmospheric and Solar-Terrestrial Physics, 64 (12-14), 1531-1543. https://doi.org/10.1016/S1364-6826(02)00091-3

[4] Zhan, W., F. S. Rodrigues, and M. A. Milla. 2018. "On the Genesis of Postmidnight Equatorial Spread F: Results for the American/ Peruvian Sector." Geophysical Research Letters 45(15): 7354-7361, https://doi.org/10.1029/2018GL078822

Acknowledgements

- The authors thank to INPE/MCTI, NSSC/CAS, COSPAR, IAGA and FAPESP for kindly support the presentation of this work.
- We gratefully thanks the Jicamarca Radio Observatory (JRO). The JRO is a facility of the Instituto Geofísico del Perú operated with support from the NSF Cooperative Agreement ATM-0432565 through Cornell University.

Results

The metric evaluation for each model is the accuracy and confusion matrix shown in Figures 6, 7, and 8. These results correspond to the test data set. Moreover, each model was applied to three RTI maps that were not used for training and testing each model. Figures 10 to 21 illustrate the comparison between the original data and each model's prediction. In addition, tables 3, 4 and 5 show the accuracy of each model.

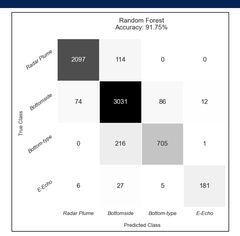

Figure 6: Confusion Matrix and accuracy of RF using test data.

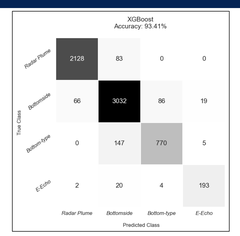

Figure 7: Confusion Matrix and accuracy of XGBoost using test data.

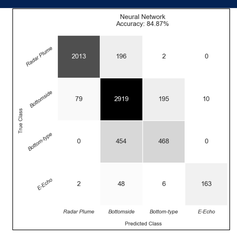

Figure 8: Confusion matrix and accuracy of NN using test data.

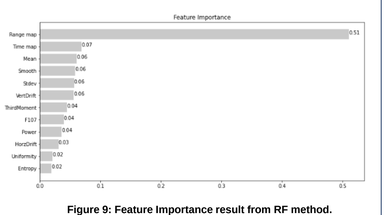

Figure 9: Feature Importance result from RF method.

Table 3: Accuracy results for RTI map measured on 29 June 2020.

MODEL	Accuracy %
RF	86.15
XGBoost	78.46
NN	46.15

Table 4: Accuracy results for RTI map measured on 6 April 2020.

MODEL	Accuracy %
RF	77.88
XGBoost	76.92
NN	49.68

Table 5: Accuracy results for RTI map measured on 3 April 2020.

MODEL	Accuracy %
RF	40.48
XGBoost	28.57
NN	88.10

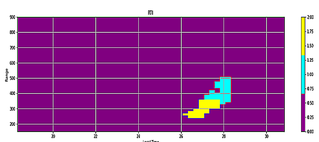

Figure 10: Original RTI map labeled.

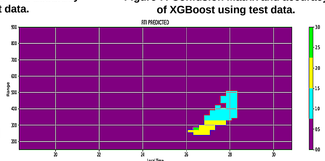

Figure 11: RF prediction.

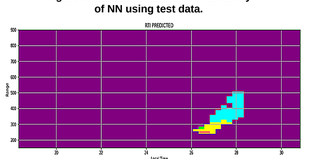

Figure 12: XGBoost prediction.

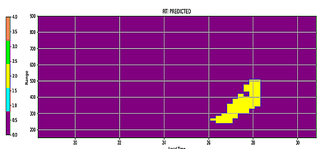

Figure 13: NN prediction.

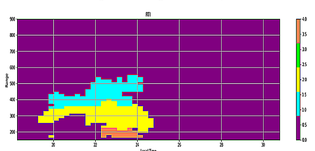

Figure 14: Original RTI map labeled.

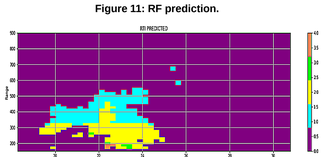

Figure 15: RF prediction.

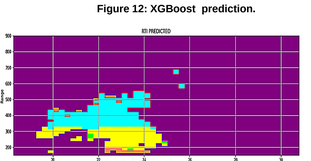

Figure 16: XGBoost prediction.

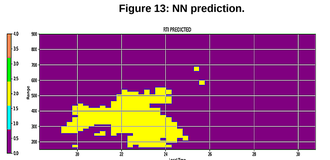

Figure 17: NN prediction.

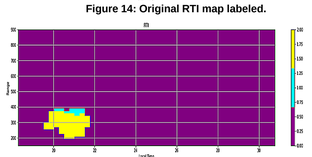

Figure 18: Original RTI map labeled.

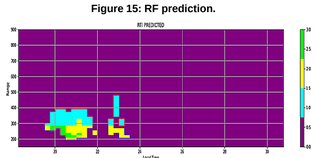

Figure 19: RF prediction.

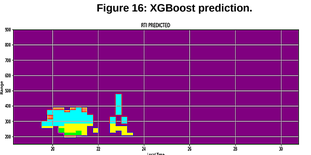

Figure 20: XGBoost prediction.

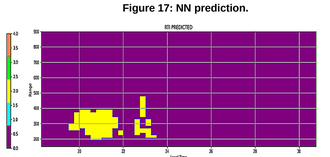

Figure 21: NN prediction.